

Phase Matching in fs BOXCARS

Dmitri Romanov^{1,2}, Aleksey Filin^{1,2}, Ryan Compton^{1,3}, Robert Levis^{1,3}

1. Center for Advanced Photonics Research, College of Science and Technology

Temple University, 1901 N. 13th Street, Philadelphia, PA 19122

2. Department of Physics, Temple University, 1900 N. 13th Street, Philadelphia, PA 19122

3. Department of Chemistry, Temple University, 1901 N. 13th Street, Philadelphia, PA 19122

We analytically describe the effect of phase matching conditions on femtosecond BOXCARS lineshape and demonstrate quantitative agreement with experimental spectra for the oxygen vibrational transition, $\Delta G_{01} = 1556.4 \text{ cm}^{-1}$.

Introduction

Phase matching is an essential component for all nonlinear conversion processes and must be taken into consideration for quantitative line shape analysis. For coherent anti-Stokes Raman scattering (CARS) a maximum in the signal intensity (resonant or nonresonant) occurs when the phase matching condition $\Delta \mathbf{k} = \mathbf{k}_{P1} + \mathbf{k}_{P2} - \mathbf{k}_S - \mathbf{k}_{CARS} = 0$ is satisfied, where \mathbf{k}_{P1} , \mathbf{k}_{P2} , \mathbf{k}_S , and \mathbf{k}_{CARS} are the wave vectors for the two pump, Stokes and CARS beams, respectively. The simplest means of achieving phase matching in CARS is through collinear beam geometry, with the \mathbf{k}_{CARS} photons generated in the same direction as the pump and Stokes beams. Phase matching conditions for the collinear configuration are increasingly relaxed as the beams

become more tightly focused into the sample [1]. Femtosecond CARS (fs-CARS) has been performed in the collinear configuration in two basic versions: (i) broadband experiments, where all beams are of fs duration [2]; (ii) multiplex experiments, where only the Stokes beam is typically of fs duration [3-6], and where many transitions can be simultaneously excited and detected. The principle drawback to collinear CARS is the necessity to filter the output signal from the input beams.

An elegant means of avoiding the inherent background from the excitation beams present in the collinear setup was developed using a BOXCARS beam geometry to impart a unique direction on \mathbf{k}_{CARS} for spatial filtering [7, 8]. Long in use in the ns and ps regimes, BOXCARS has recently become an important tool for experiments requiring fs time resolution, for instance, in measurements of temperature [9-12], rotational and vibrational constants [9, 10], and wavepacket dynamics [13].

In the fs pulse regime, the BOXCARS beam geometry does not afford the same simplicity in phase matching as does the collinear geometry [1]. An appreciable wave vector mismatch occurs between the various frequency components within the fs pulses due to the broad bandwidth and noncollinearities. This necessitates a detailed analysis of the phase matching conditions, because no practical experimental means exists to compensate for the wave vector mismatch in fs BOXCARS. In this letter we present a theoretical description that accounts for the broad bandwidth of the fs pulses and the corresponding phase matching effects on fs-BOXCARS. This theory is compared to experiments on O₂.

Theory

We will consider the phase matching conditions for fs BOXCARS as outlined in the inset to Figure 1. The two pump beams of frequency ω_p that impinge the focusing lens (L1) lie in the horizontal plane and are separated by a distance d ; the Stokes beam of frequency ω_s is incident at a distance h above the plane of the pump beams. Both L1 and L2 lenses have the same focal distance, f .

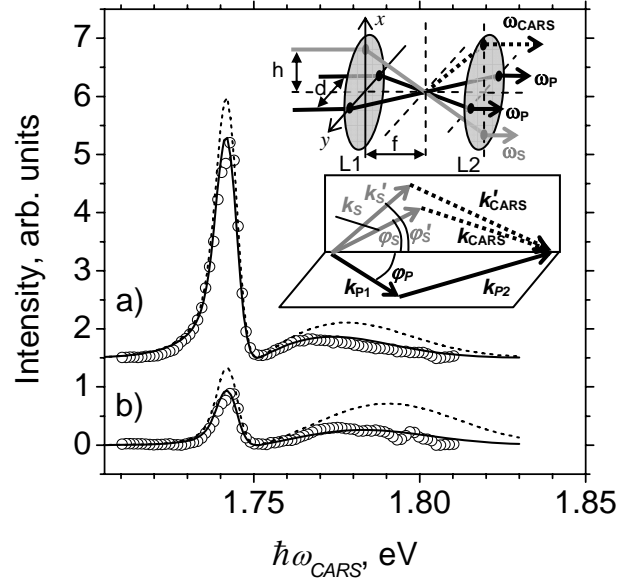


Fig.1. Typical dependence of CARS signal intensity on CARS photon energy for two different Stokes photon energies in fs BOXCARS experiment. Circles represent the experiment, dashed line – the theory without a correction on phase mismatch, solid line – the theory with the correction. The inset shows the beam geometry for folded BOXCARS and phase-matching conditions for fs BOXCARS (see details in the text)

The finite diameter of the beams ($2r_0$) and finite duration of the pulses are two major sources of phase mismatch in fs BOXCARS. The finite diameter leads to mismatch

of the directions of the participating wavevectors \mathbf{k}_s and \mathbf{k}'_s shown in the inset to Fig. 1. This detuning of the Stokes wavevector as a function of angle is $\sim r_0/h$. The finite (and short) temporal duration of the pulses leads to a relatively broad frequency distribution and thus causes considerable detuning of the wavevector magnitudes within a given laser pulse. For the same Stokes beam, this detuning is $\sim \delta\omega_s / c\omega_s$. The phase mismatch tolerance to the frequency deviations and the corresponding phase mismatch attenuation of the output CARS signal will be determined by the interaction length and the transverse beam profiles.

To account for CARS output signal distortion due to phase mismatching, we assume that the system is tuned to achieve perfect phase match for infinitely narrow beams and that the beam frequencies satisfy $\omega_{p1} = \omega_{p2} = \omega_{p0}$ and $\omega_s = \omega_{s0}$. In this case, the energy and momentum conservation rules, $\omega_{p1} + \omega_{p2} - \omega_s = \omega_{CARS}$ and $\mathbf{k}_{p1} + \mathbf{k}_{p2} - \mathbf{k}_s = \mathbf{k}_{CARS}$, stipulate the following relation between φ_{s0} and φ_{p0} , the angles of incidence for the excitation beams at the focal spot (see the inset in Fig. 1):

$$\tan(\varphi_{s0}) = \frac{\tan(\varphi_{p0})}{\sqrt{g}}; \quad g = \left(2 \frac{\omega_{p0}}{\omega_{s0}} - 1\right)^{-1} \quad (1)$$

Small deviations of the frequencies and the angles from their phase-matching values bring about the phase mismatch in the CARS wavevector. Let us assume that in the plane of the lens LI in Fig. 1, the three beams are centered at the points satisfying the conditions of Eq. (1); the beams have transverse Gaussian shape with the same diameter $2r_0 \ll d, h$ and small frequency deviations, $\delta\omega_s = \omega_s - \omega_{s0}$, $\delta\omega_{p1} = \omega_{p1} - \omega_{p0}$, and $\delta\omega_{p2} = \omega_{p2} - \omega_{p0}$. Then, for the portions of these beams that have the local Cartesian

coordinates x_i, y_i ($i = S, P1, P2$) measured from the respective beam center, the amount of the wavevector mismatch is obtained as,

$$\delta k_{CARS} = \frac{\omega_{P0}}{c} \frac{d}{2} \left(\sqrt{g} (x_1 + x_2 - 2x_3) + (y_1 - y_2) - \frac{d}{2} \frac{g+1}{2} \frac{\omega_{P0}}{\omega_{S0}} \left(2 \frac{\delta\omega_S}{\omega_{S0}} - \frac{\delta\omega_{P1} + \delta\omega_{P2}}{\omega_{P0}} \right) \right), (2)$$

to the first order of the small parameters, $|x_i/f|$ and $|\delta\omega_i/\omega_{i0}|$. This correction leads to the relative suppression of the CARS output through the spatial mismatch attenuation factor, $G(\delta\omega_{P1}, \delta\omega_{P2}, \delta\omega_S)$, produced by the averaging of the usual factor, $\sin^2(l\delta k_{CARS})/(l\delta k_{CARS})^2$, with the Gaussian profiles of the three beams and thus determined by the interplay of the effective interaction length, l , and the transverse distribution width of the pump and Stokes beams, r_0 .

For the small-angle experiment setup considered here, l is approximately found as the intersection of the three Gaussian beams in the focal region. The sine function is fast-oscillating on the r_0 scale; thus we can approximate the averaging integral and obtain (for $\omega_{P1} = \omega_{P2}$) the following simplified expression for the mismatch attenuation factor:

$$G(\omega_{CARS}, \omega_S) = \frac{1}{r_0 \sqrt{2\pi(1+3g)}} \exp \left(- \left(\frac{d}{2r_0} \right)^2 \frac{(g+1)^2}{2(1+3g)} \frac{1}{(2\omega_{P0})^2} \left(\frac{\omega_S}{g} - \omega_{CARS} \right)^2 \right) \quad (3)$$

where d is the distance between the two pump beams on the focusing lens and $g = \omega_{RES}/(2\omega_P - \omega_{RES})$.

Experimental setup

A 50 fs Ti:sapphire regenerative amplifier was used to generate pump pulses centered at 800 nm with a 425 fs pulse duration and 1 kHz repetition rate and to pump the

optical parametric amplifier (OPA) generating the 140 fs Stokes. The OPA was scanned to provide all the necessary Stokes frequencies. The excitation beams were focused ($f = 25$ cm) into an optical chamber to measure a spectrum of oxygen (300 K, 1 Atm.)

Results and discussion

Figure 1 displays measurements of spectrally-resolved fs BOXCARS signal collected with the Stokes photon energy detuned from resonance for a) 28 meV and b) 44 meV (corresponding to $\hbar\omega_{s_0} = 1.385$ eV and $\hbar\omega_{s_0} = 1.401$ eV, respectively, with the resonance condition occurring at $\hbar\omega_{s_0} = 1.357$ eV.). The experimental measurements (circles) for the oxygen vibrational transition $\Delta G_{01} = 1556.4$ cm^{-1} (that is $\hbar\omega_{p_0} - \hbar\omega_{s_0} = 193$ meV) display a peak centered at $\hbar\omega_{\text{CARS}} = 1.743$ eV for the resonant signal with a spectral position independent of $\hbar\omega_{s_0}$. The broad peak in each spectrum corresponds to the nonresonant contribution (with position dependent upon $\hbar\omega_{s_0}$).

In a simple collinear geometry, the dependence of the emitted CARS signal on the CARS and Stokes frequencies, at a fixed frequency of the pump beam, can be describe by a model theoretical curve [14],

$$I_{\text{CARS}}(\omega_{\text{CARS}}, \omega_S) = I_0 e^{-\frac{(1+\alpha)(\omega_{\text{CARS}} + \omega_S - 2\omega_P)^2}{(2+\alpha)^2 \sigma}} \left| \beta + i e^{-\frac{-(\omega_F)^2}{2\sigma}} \left(1 + \text{Erf} \left(\frac{i\omega_F}{\sqrt{2\sigma}} \right) \right) \right|^2, \quad (4)$$

where $\omega_F = ((2+\alpha)\Omega + \omega_S + \alpha\omega_P - (1+\alpha)\omega_{\text{CARS}})/(2+\alpha)$; the parameters σ and α are given by the pump and Stokes linewidths: $\sigma = (1+\alpha)(FWHM_p)^2 / ((2+\alpha)4\ln 2)$, $\alpha = (FWHM_s / FWHM_p)^2$. In Fig. 1, the dashed curve corresponds to a fit using Eq. (4) without taking into account the geometrical phase mismatch that occurs for each Stokes

photon energy. The solid curve is a fit using of Eqs. (4) and (3), including the geometrical phase matching correction. Only two fitting parameters, I_0 and β , were used to create the theoretical curves. I_0 represents the maximum intensity of the CARS signal given a particular experimental arrangement and β represents the ratio of resonant to nonresonant signal. The remaining parameters were taken from experiment. Fig. 1 depicts the significant discrepancy between theory and experiment when the geometrical phase matching condition is ignored. Without the correction, the peak in the resonant and nonresonant signal in both spectra far exceeds that in the experimental data.

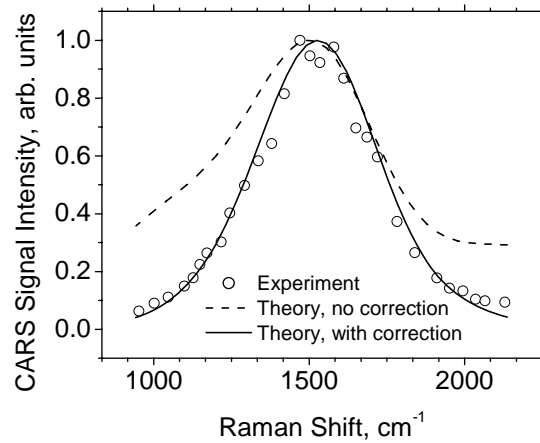


Fig. 2. CARS spectrum of the oxygen vibrational transition $\Delta G_{01} = 1556.4 \text{ cm}^{-1}$. Circles represent the experiment, dashed line – the theory without a correction on phase mismatch, solid line – the theory with the correction.

Fig. 2 shows the CARS spectrum of the fundamental vibrational transition of oxygen at $\Delta G_{01} = 1556.4 \text{ cm}^{-1}$. Theoretical curves were simulated using the same set of parameters, as in Fig. 1. The experimental and theoretical curves were generated by

integrating over the CARS photon energy (integrating the curves as depicted in Fig. 1 for all values of Stokes detuning). The experimental data (circles) generates a line shape that differs significantly from that expected due to ns CARS. That is, the nonresonant background should not diminish to zero at large Stokes detunings, but should rather level off to some constant value that is independent of the Raman shift due to nonresonant electronic polarization, according to Eq. (4). The theoretical curve without phase mismatch correction (dashed line) predicts that the nonresonant contribution to the signal to remain constant with large detuning. Upon application of Eq. (3), the theoretical curve (solid line) is in excellent agreement with the experimental data.

Conclusion

It has been shown, that for correct analysis of the data taken in fs BOXCARS it is necessary to take into account the phase matching conditions to accurately model both the linshape of emitted CARS signal and the CARS spectrum generated from the CARS signal as a function of Stokes wavelength. The appropriate phase matching correction was developed theoretically and the theoretical predictions are in good agreement with experiment.

Acknowledgements

This work is supported by DARPA.

References

1. G. C. Bjorklund, IEEE J. Quantum Electron. **QE-11**, 287 (1975).
2. A. Zumbusch, G. R. Holtom, and X. S. Xie, Phys. Rev. Lett. **82**, 4142 (1999).
3. J.-X. Cheng *et al.*, J. Phys. Chem. B **106**, 8493 (2002).
4. N. Dudovich, D. Oron, and Y. Silberberg, J. Chem. Phys **118**, 9208 (2003).
5. D. Oron, N. Dudovich, and Y. Silberberg, Phys. Rev. Lett. **90**, 213902 (2003).
6. H. Kano and H. Hamaguchi, Appl. Phys. Lett. **85**, 4298 (2004).
7. A. C. Eckbreth, Appl. Phys. Lett. **32**, 421 (1978).
8. Y. Prior, Appl. Optics **19**, 1741 (1980).
9. T. Lang, K.-L. Kompa, M. Motzkus, Chem. Phys. Lett. **310**, 65 (1999).
10. P. Beaud, H.-M. Frey, T. Lang, M. Motzkus, Chem. Phys. Lett. **344**, 407 (2001).
11. T. Lang, M. Motzkus, J. Opt. Soc. Am. B **19**, 340 (2002).
12. R. P. Lucht, *et al.*, Appl. Phys. Lett. **89**, 251112 (2006).
13. M. Schmitt *et al.*, Chem. Phys. Lett. **270**, 9 (1997).
14. R. Compton *et al.*, submitted to PRL (2007)

References with Titles

1. G. C. Bjorklund, Effects of focusing on third-order nonlinear process in isotropic media, *IEEE J. Quantum Electron.* **QE-11**, 287 (1975).
2. A. Zumbusch, G. R. Holtom, and X. S. Xie, Three-Dimensional Vibrational Imaging by Coherent Anti-Stokes Raman Scattering, *Phys. Rev. Lett.* **82**, 4142 (1999).
3. J.-X. Cheng *et al.*, Multiplex Coherent Anti-Stokes Raman Scattering Microspectroscopy and Study of Lipid Vesicles, *J. Phys. Chem. B* **106**, 8493 (2002).
4. N. Dudovich, D. Oron, and Y. Silberberg, Single-pulse coherent anti-Stokes Raman spectroscopy in the fingerprint spectral region, *J. Chem. Phys.* **118**, 9208 (2003).
5. D. Oron, N. Dudovich, and Y. Silberberg, Femtosecond phase-and-polarization control for background-free coherent anti-Stokes Raman spectroscopy, *Phys. Rev. Lett.* **90**, 213902 (2003).
6. H. Kano and H. Hamaguchi, Femtosecond coherent anti-Stokes Raman scattering spectroscopy using supercontinuum generated from a photonic crystal fiber, *Appl. Phys. Lett.* **85**, 4298 (2004).
7. A. C. Eckbreth, BOXCARS: Crossed-beam phase-matched CARS generation in gases, *Appl. Phys. Lett.* **32**, 421 (1978).
8. Y. Prior, Three-dimensional phase matching in four-wave mixing, *Appl. Optics* **19**, 1741 (1980).

9. T. Lang, K.-L. Kompa, Femtosecond CARS on H₂, M. Motzkus, Chem. Phys. Lett. **310**, 65 (1999).
10. P. Beaud *et al.*, Flame thermometry by femtosecond CARS. Chem. Phys. Lett. **344**, 407 (2001).
11. T. Lang, M. Motzkus, Single-shot femtosecond coherent anti-Stokes Raman-scattering thermometry, J. Opt. Soc. Am. B **19**, 340 (2002).
12. R. P. Lucht, *et al.*, Femtosecond coherent anti-Stokes Raman scattering measurement of gas temperatures from frequency-spread dephasing of the Raman coherence, Appl. Phys. Lett. **89**, 251112 (2006).
13. M. Schmitt *et al.*, Femtosecond time-resolved coherent anti-Stokes Raman scattering for the simultaneous study of ultrafast ground and excited state dynamics: iodine vapour, Chem. Phys. Lett. **270**, 9 (1997).
14. R. Compton *et al.*, Elucidating the Spectral and Temporal Contributions from the Resonant and Nonresonant Response to fs CARS, submitted to PRL (2007)